

Optimization of the grain boundary diffusion process by doping gallium and zirconium in Nd-Fe-B sintered magnets

Zhiteng Li(李之藤), Haibo Xu(徐海波), Feng Liu(刘峰), Rongshun Lai(赖荣舜), Renjie Wu(武仁杰),Zhibin Li(李志彬), Yangyang Zhang(张洋洋), and Qiang Ma(马强)
Citation: Chin. Phys. B, 2023, 32 (**10**): 107503. DOI: 10.1088/1674-1056/acd61f
Journal homepage: http://cpb.iphy.ac.cn; http://iopscience.iop.org/cpb

What follows is a list of articles you may be interested in

Effect of TbF_3 diffusion on the demagnetization behavior and domain evolution of sintered Nd-Fe-B magnets by electrophoretic deposition

Xue-Jing Cao(曹学静), Shuai Guo(郭帅), Yu-Heng Xie(谢宇恒), Lei Jin(金磊), Guang-Fei Ding(丁广飞),Bo Zheng(郑波), Ren-Jie Chen(陈仁杰), and A-Ru Yan(闫阿儒)
Chin. Phys. B, 2023, 32 (**9**): 097503. DOI: 10.1088/1674-1056/acaf2d

Effects of post-sinter annealing on microstructure and magnetic properties of Nd-Fe-B sintered magnets with Nd-Ga intergranular addition

Jin-Hao Zhu(朱金豪), Lei Jin(金磊), Zhe-Huan Jin(金哲欢), Guang-Fei Ding(丁广飞), Bo Zheng(郑波), Shuai Guo(郭帅), Ren-Jie Chen(陈仁杰), and A-Ru Yan(闫阿儒)
Chin. Phys. B, 2021, 30 (**6**): 067503. DOI: 10.1088/1674-1056/abddad

Progress in recycling of Nd-Fe-B sintered magnet wastes

Ming Yue(岳明), Xiaowen Yin(尹小文), Weiqiang Liu(刘卫强), Qingmei Lu(路清梅)
Chin. Phys. B, 2019, 28 (**7**): 077506. DOI: 10.1088/1674-1056/28/7/077506

Magnetic properties of misch-metal partially substituted Nd-Fe-B magnets sintered by dual alloy method

Jie-Fu Xiong(熊杰夫), Rong-Xiang Shang(商荣翔), Yan-Li Liu(刘艳丽), Xin Zhao(赵鑫), Wen-Liang Zuo(左文亮), Feng-Xia Hu(胡凤霞), Ji-Rong Sun(孙继荣), Tong-Yun Zhao(赵同云), Ren-Jie Chen(陈仁杰), Bao-Gen Shen(沈保根)
Chin. Phys. B, 2018, 27 (**7**): 077504. DOI: 10.1088/1674-1056/27/7/077504

Effects of oxidation of DyH_3 in Nd-Fe-B sintered magnets

Yan Gao-Lin (严高林), Fang Zhi-Hao (方之颢)
Chin. Phys. B, 2015, 24 (**10**): 107503. DOI: 10.1088/1674-1056/24/10/107503

Optimization of the grain boundary diffusion process by doping gallium and zirconium in Nd–Fe–B sintered magnets

Zhiteng Li(李之藤)[1,2], Haibo Xu(徐海波)[2], Feng Liu(刘峰)[3], Rongshun Lai(赖荣舜)[1,2], Renjie Wu(武仁杰)[2], Zhibin Li(李志彬)[2], Yangyang Zhang(张洋洋)[1,2], and Qiang Ma(马强)[1,2,†]

[1] *School of Rare Earths, University of Science and Technology of China, Hefei* 230026, *China*
[2] *Ganjiang Innovation Academy, Chinese Academy of Sciences, Ganzhou* 341000, *China*
[3] *Baotou Yunsheng Strong Magnet Material Co., LTD, Baotou* 014000, *China*

(Received 7 February 2023; revised manuscript received 15 May 2023; accepted manuscript online 17 May 2023)

As the channel for grain boundary diffusion (GBD) in Nd–Fe–B magnets, grain boundary (GB) phases have a very important effect on GBD. As doping elements that are commonly used to regulate the GB phases in Nd–Fe–B sintered magnets, the influences of Ga and Zr on GBD were investigated in this work. The results show that the Zr-doped magnet has the highest coercivity increment (7.97 kOe) by GBD, which is almost twice that of the Ga-doped magnet (4.32 kOe) and the magnet without Ga and Zr (3.24 kOe). Microstructure analysis shows that ZrB_2 formed in the Zr-doped magnet plays a key role in increasing the diffusion depth. A continuous diffusion channel in the magnet can form because of the presence of ZrB_2. ZrB_2 can also increase the defect concentration in GB phases, which can facilitate GBD. Although Ga can also improve the diffusion depth, its effect is not very obvious. The micromagnetic simulation based on the experimental results also proves that the distribution of Tb in the Zr-doped magnet after GBD is beneficial to coercivity. This study reveals that the doping elements Ga and Zr in Nd–Fe–B play an important role in GBD, and could provide a new perspective for researchers to improve the effects of GBD.

Keywords: Nd–Fe–B sintered magnet, ZrB_2 phase, grain boundary diffusion, micromagnetic simulation

PACS: 75.50.Ww, 75.50.Vv, 75.78.Cd, 75.20.En **DOI:** 10.1088/1674-1056/acd61f

1. Introduction

The Nd–Fe–B alloy has been the most excellent magnet since it was invented by Sagawa *et al.*[1] In recent years, the rapid development of electric vehicles[2] has brought large demand for Nd–Fe–B magnets with high coercivity. Therefore, coercivity enhancement is a focus of Nd–Fe–B research. Substitution of heavy rare earth (HRE) elements, such as Tb/Dy, for Nd is a conventional strategy that is used to enhance the coercivity of Nd–Fe–B magnets, because of the higher anisotropy field (H_A) of $(Tb/Dy)_2Fe_{14}B$ than that of $Nd_2Fe_{14}B$.[3,4] However, the magnetic moments of the Tb/Dy and Fe atoms are antiparallel,[4,5] which causes a significant decrease in remanence (B_r).

In 2000, Park *et al.*[6] deposited Dy film on a sintered Nd–Fe–B magnet followed by heat treatment, which is the genesis of the grain boundary diffusion (GBD) process. During the GBD process, Tb/Dy atoms diffuse from the surface into the magnet through GB phases, and a core–shell structure is formed.[7,8] The coercivity mechanism of sintered Nd–Fe–B is generally considered as a nucleation mechanism,[9] and the defects and corners of the grains make it easy for the demagnetization domain to nucleate.[10] The higher H_A of the shell can inhibit the nucleation at the grain surface and the thicker GB phase layers formed by GBD also contribute greatly to coercivity.[11,12] Compared with the addition of Tb/Dy, the decrease in remanence is much smaller.

However, the coercivity increment by GBD tends to decrease when the magnet thickness increases.[13] Therefore, researchers have put considerable effort into increasing the depth of diffusion. At present, a lot of research is concerned with the development of diffusion sources, which can be divided into three types,[14] including HRE-based,[15–17] light rare-earth-based[18–21] and non rare earth based[22–24] diffusion sources. In addition to the diffusion sources, studies showed that the compositions in magnets have important effects on GBD. Bae *et al.*[25] reported that oxygen has a negative effect on GBD. A lower Al content in the magnet was found to be beneficial to GBD by Diao *et al.*[26] And Zhong *et al.*[27] found that the Ti element in the Nd–Fe–B has a positive effect on GBD. However, research on the influence of the magnet on GBD is still insufficient. To gain a comprehensive understanding of GBD, it is necessary to determine how the magnet itself influences GBD.

Ga and Zr are commonly used doping elements in Nd–Fe–B, which have been well studied.[28,29] Ga doping can improve the wettability of the Nd-rich phase to form a continuous GB layer,[9,30,31] and Zr doping can refine the grains by pinning in GB phases.[32] The main purpose of Ga and Zr doping is to optimize the GB phases and microstructure of magnets, and Xu *et al.*[33] reported that GB phases play an important role in GBD. Ga and Zr doping may have some effects on

†Corresponding author. E-mail: maqiang5019@126.com

© 2023 Chinese Physical Society and IOP Publishing Ltd

GBD, but they are still unknown. To optimize GBD, a comprehensive study of the factors that may affect GBD is necessary. Therefore, it is worth studying the influence of these two doping elements on GBD.

In the field of permanent magnets, micromagnetic simulation is an effective way to study the relationship between microstructures and magnetic properties.[34–36] In this paper, micromagnetic simulation was used to further analyze the different structures of the magnet based on the experiment.

2. Experimental and simulation methods

2.1. Sample preparation and characterization

Three kinds of samples with the compositions of

$$(Pr,Nd)_{31}Cu_{0.2}Al_{0.1}Co_1Fe_{bal}B_{0.94},$$
$$(Pr,Nd)_{31}Cu_{0.2}Al_{0.1}Ga_{0.5}Co_1Fe_{bal}B_{0.94},$$
$$(Pr,Nd)_{31}Cu_{0.2}Al_{0.1}Zr_{0.5}Co_1Fe_{bal}B_{0.94}$$

were prepared via a powder metallurgical process, including strip-casting, hydrogen decrepitation and jet milling. The median particle sizes were controlled to about 3.7 μm for all samples. The fine powders were compressed and oriented under a 2.0 T magnetic field, followed by isostatic pressing at 195 MPa. Next, the green compacts were sintered (1030 °C–1080 °C) and annealed (900 °C for 1st and 500 °C–600 °C for 2nd) at their respective optimal temperatures to achieve the optimum magnetic properties. These samples before GBD were marked as original, Ga-doped and Zr-doped, respectively. The magnets before GBD were cut into cylinders with a size of $\varphi 10 \times 6$ mm. The samples were polished and then washed in distilled water ultrasonically. Next, the magnets were acidized in 3% nitric acid for 50 s. Then, the magnets were cleaned with distilled water and alcohol ultrasonically. Subsequently, all the magnets were covered by Tb film via a magnetron sputtering system. A commercial Tb target (99.9%, Hefei Kejing Materials Technology Co., Ltd.) was used to fabricate the diffusion source. During the deposition, the argon pressure was maintained at 1 Pa, and the direct current power was set to 120 W. The film weights were controlled at 0.42 wt% of the magnet for all the samples. All three magnets were then treated at 900 °C for 6 h in vacuum, and annealed at the optimal temperature (500 °C) for 3 h in vacuum. Samples after GBD were marked as original GBD, Ga-doped GBD and Zr-doped GBD, respectively.

The magnetic properties of the samples were measured by a B–H tracer (NIM-500C). The microstructures of the samples were observed using a backscattered electron scanning electronic microscope (BSE-SEM) (JEOL JSM 7200F). The element distributions were obtained via electron probe micro analysis (Shimadzu EPMA-1720H). The crystal structure of micro-areas in the triangular junction phase (TJP) was characterized using transmission electron microscopy (TEM, FEI Tecnai G2 F20).

2.2. Micromagnetic simulation

The parallel finite element micromagnetic package Magpar[37] was used for micromagnetic simulation to understand the effect of Tb-rich shell thickness on coercivity. In this work, a model with a polycrystalline microstructure based on Voronoi tessellation[38] was established by Neper[39] and Gmsh.[40] This model was a cube with a size of 300 nm × 300 nm × 300 nm containing 27 irregular grains, as shown in Fig. 1. Due to the limitation of computing capability, the grain size in this model was smaller than the actual grain size. In addition, the model consisted of three parts, namely, the core of $Nd_2Fe_{14}B$, the shell of $(Tb_{0.25}Nd_{0.75})_2Fe_{14}B$, and the GB phases. All the grains were surrounded by a Tb-rich shell and separated by GB phases. The width of the GB was set to about 5nm. The influence of the shell thickness on coercivity was studied by changing the shell thickness from 0 nm to 10 nm. The material parameters of $Nd_2Fe_{14}B$ and $Tb_2Fe_{14}B$ were taken from the literature.[4,41] The saturation magnetic polarizations (J_S) were 1.61 T and 0.7 T for $Nd_2Fe_{14}B$ and $Tb_2Fe_{14}B$. The anisotropy constants (K_1) were 4.5 MJ/m^3 and 5.9 MJ/m^3 for $Nd_2Fe_{14}B$ and $Tb_2Fe_{14}B$. And the exchange stiffness (A) was 12.5 pJ/m and 13.3 pJ/m for $Nd_2Fe_{14}B$ and $Tb_2Fe_{14}B$. The magnetic properties for the GB phases were defined as amorphous soft magnetic phases[15] and J_S, K_1, and A were 0.15 T, 0 MJ/m^3, and 5 pJ/m, respectively. The magnetic parameters for $(Tb_{0.25}Nd_{0.75})_2Fe_{14}B$ were obtained by linear interpolation.

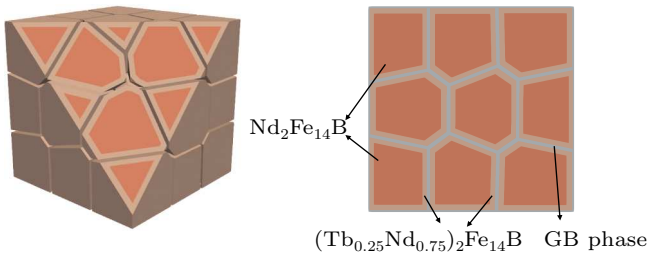


Fig. 1. The polycrystalline model with a size of 300 nm × 300 nm × 300 nm, containing 27 irregular grains with a core-shell structure.

3. Results and discussion

3.1. Magnetic properties

Figure 2 shows the demagnetization curves and the comparison of the coercivity of the samples with different doping elements before and after GBD. The detailed magnetic properties are listed in Table 1. With Ga or Zr doping, the coercivity decreases slightly from 14.38 kOe to 13.41 kOe or 13.63 kOe, respectively. The decrease in magnetic properties may be due to the excessive addition of Ga or Zr.[42,43] The coercivities

of the three GBD samples are all enhanced significantly after diffusion, but the coercivity increments of the three samples are quite different, as shown in Fig. 2(b). The coercivity of the original magnet increases by only 23% through GBD, from 14.38 kOe to 17.62 kOe. The coercivity increment of the Ga-doped magnet is slightly higher, increasing by 32% from 13.41 kOe to 17.73 kOe. In contrast, the coercivity increment for the Zr-doped magnet is 7.97 kOe, increasing by 58% from 13.63 kOe to 21.60 kOe, which is quite huge for a magnet with a thickness of 6 mm. The results show that both Ga and Zr have a positive effect on GBD, but the effect of Zr is particularly significant.

Table 1. The magnetic properties of the six different magnets.

Sample	B_r (kGs)	H_{cj} (kOe)	$(BH)_{max}$ (MGOe)	ΔH_{cj} (kOe)
Original	14.14	14.38	48.74	–
Original GBD	14.08	17.62	48.71	3.24
Ga-doped	13.99	13.41	47.41	–
Ga-doped GBD	13.88	17.73	47.17	4.32
Zr-doped	14.01	13.63	46.84	–
Zr-doped GBD	13.92	21.60	47.80	7.97

The performances of the GBD samples at high temperatures were also measured, as shown in Fig. 3. The temperature coefficients of remanence (α) and coercivity (β) in the range of T to T_i are calculated by the following equations:[44]

$$\alpha = \frac{B_r(T_i) - B_r(T_0)}{B_r(T_0)(T_i - T_0)} \times 100\%, \tag{1}$$

$$\beta = \frac{H_{cj}(T_i) - H_{cj}(T_0)}{H_{cj}(T_0)(T_i - T_0)} \times 100\%. \tag{2}$$

The temperature coefficient of remanence of the Ga-doped and Zr-doped GBD magnets decreases slightly compared with the original GBD magnet, from -0.104 %/°C to -0.107 %/°C and -106 %/°C, respectively. However, it can be found that the temperature coefficient of coercivity of the Zr-doped GBD magnet increases significantly to -0.530 %/°C, while it is only -0.622 %/°C and -0.630 %/°C for the original GBD magnet and Ga-doped GBD magnet. The results show that the demagnetization resistance of the Zr-doped GBD magnet at high temperature is greatly improved compared with the other two samples, which can be used in high-temperature applications.

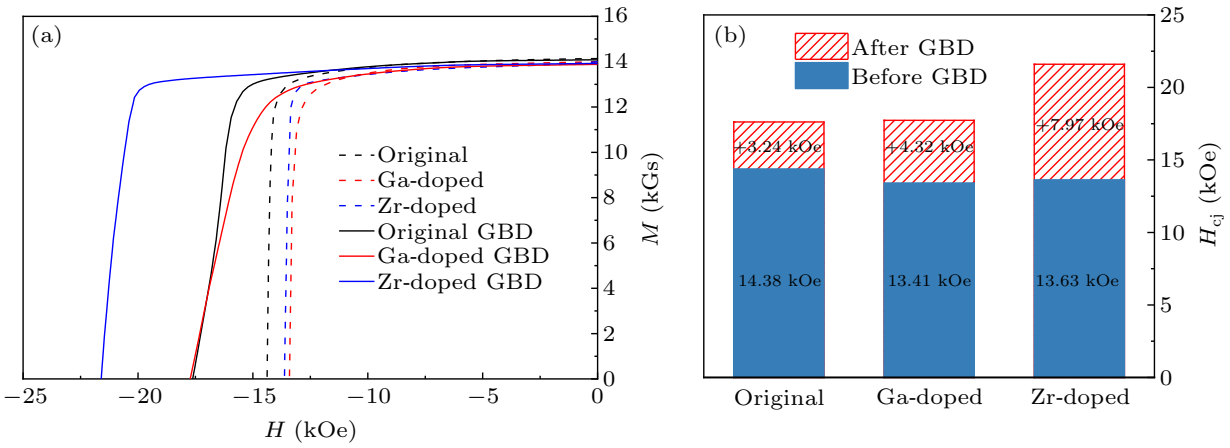


Fig. 2. (a) Demagnetization curves and (b) the coercivity comparison of the original, Ga-doped and Zr-doped magnets before and after GBD at room temperature.

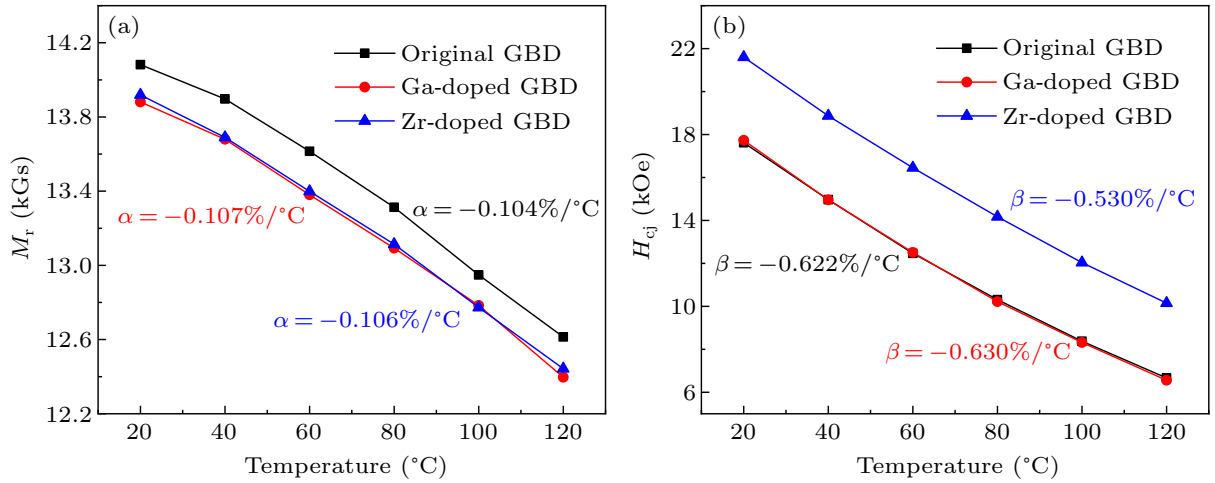


Fig. 3. The temperature dependence of remanence (a) and coercivity (b) of the original GBD magnet, Ga-doped GBD magnet and Zr-doped GBD magnet.

3.2. Microstructure characterization and analysis

The literature indicates that the coercivity increment by GBD is derived from the Tb-rich shell and the optimization of GB phases.[12] It implies that the Ga or Zr doping may have influences on the optimization of the Tb-rich shell structure or GB phase. Therefore, the microstructure evolution of magnets doped with different elements before and after GBD was analyzed to explore the reason for the differences in the coercivity increments. Figure 4 shows the BSE-SEM images of three samples before and after GBD. There are three different contrast areas, white, dark gray and light gray, which respectively represent the GB phases, (Pr, Nd)$_2$Fe$_{14}$B main phases, and (Tb, Pr, Nd)$_2$Fe$_{14}$B shells. It can be found in Fig. 4(i) that there are some regions with different contrasts in the TJP (circled in red), which may be a new phase due to the addition of Zr. Figures 4(b), 4(f), and 4(j) display the morphologies of the corresponding three magnets after GBD at the depth of 20 μm, respectively. Core-shell structures can be observed in all three magnets. For all three magnets after GBD, the shell thickness decreases with the increase in diffusion depth. It is also hard to observe the clearly visible shells in the original GBD and Ga-doped GBD magnets (Figs. 4(c) and 4(g)) at the depth of 100 μm. However, it is very interesting that there are still many thin shells in the Zr-doped GBD magnet at a depth of 100 μm, and the shells were more uniform. Even at a depth of 200 μm, there are still thin shells on the surface of some grains, as shown in Fig. 4(l). In contrast, Tb-rich shells almost completely disappear and the GB phase is discontinuous in the original GBD and Ga-doped GBD magnets at the depth of 200 μm. This means that there is more uniform distribution in the depth of Tb in the Zr-doped GBD magnet. It is worth noting that the shell thickness on the surface of the magnet decreases with the increase in the diffusion depth, as shown in Figs. 4(b), 4(f), and 4(j). The shells around the main phase in Figs. 4(b) and 4(f) are much thicker with 2 μm. But the shell thickness in Fig. 4(j) is only about 0.7 μm. Therefore, the difference in the coercivity increment by GBD of the three magnets can mainly be attributed to the distribution of Tb atoms.

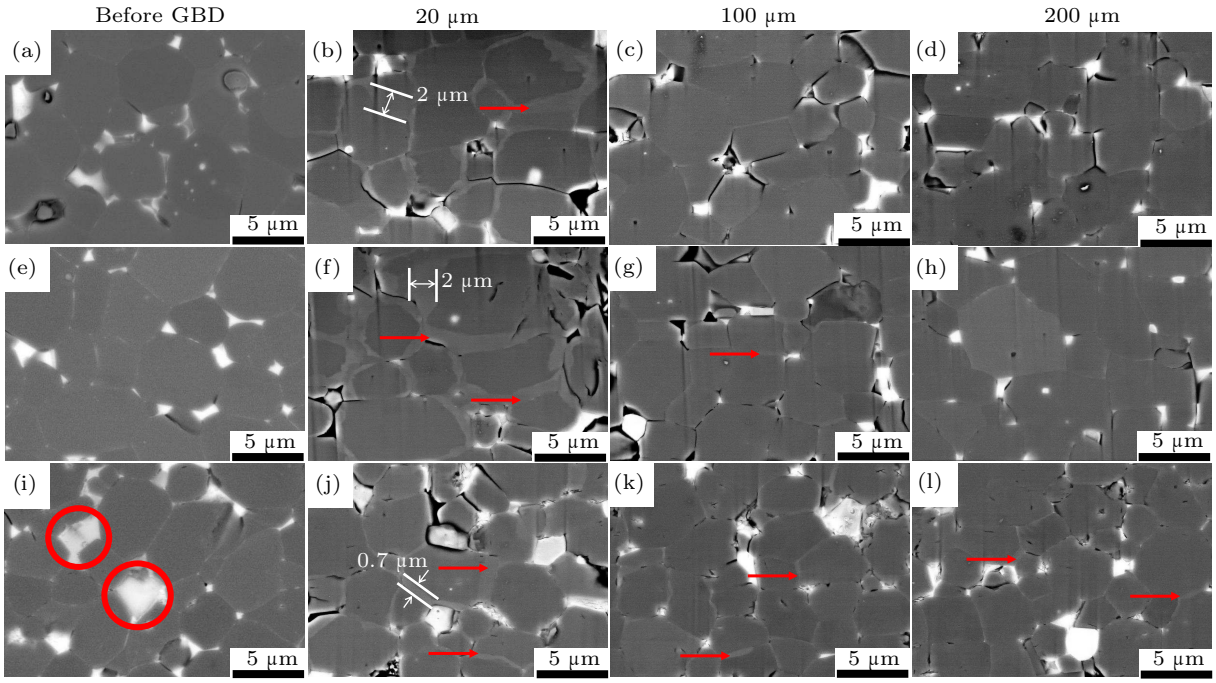


Fig. 4. BSE-SEM images of the original magnet (a), the Ga-doped magnet (e), the Zr-doped magnet (i) and original GBD magnet (b)–(d), the Ga-doped GBD magnet (f)–(h), and the Zr-doped GBD magnet (j)–(l) at depths of 20 μm, 100 μm, and 200 μm.

To more accurately describe the Tb distribution of the three magnets after GBD, EPMA characterization was carried out, as shown in Fig. 5. The results show that Tb atoms are enriched on the surface of the magnet. With the increase in depth, the proportion of the Tb-rich area and the concentration of Tb drop significantly. According to Fick's law, the concentration gradient is the main driving force for diffusion. Therefore, the decrease in the Tb concentration gradient with the increase in depth is the main reason. When the depth exceeds 100 μm, Tb elements are difficult to detect in the original GBD magnet. In contrast, Tb elements can still be observed in relatively low concentrations at the depth from 100 μm to 200 μm in the Ga-doped GBD magnet, but the green relatively low-concentration Tb area basically disappears when the diffusion depth exceeds 200 μm, as shown in Fig. 5(b). In particular, in Zr-doped GBD magnets, when the depth exceeds 200 μm, the distribution of the green relatively low-concentration Tb area can still be detected, as shown in Fig. 5(c). Moreover, the

uniformity of the Tb distribution in the Zr-doped GBD magnet is significantly improved. Both the diffusion depth and distribution uniformity of the Tb elements are consistent with the increment of coercivity for GBD magnets. Accordingly, the Tb element distribution and diffusion depth shown by EPMA agree with the results of BSE-SEM.

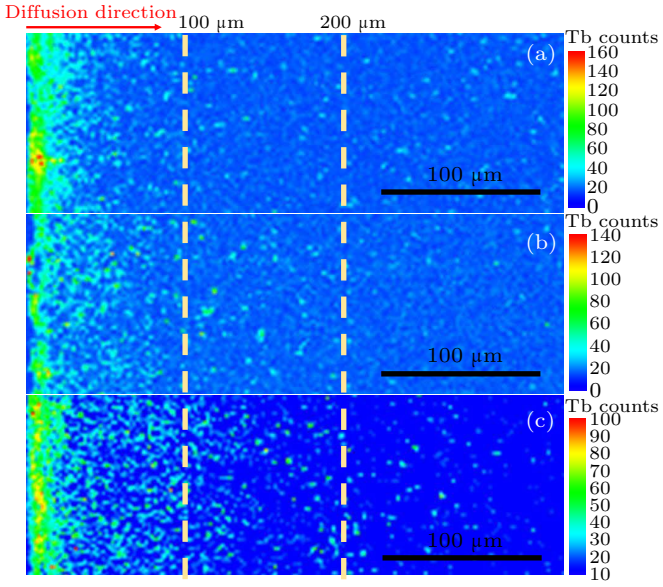


Fig. 5. EPMA mappings of Tb in the original magnet (a), the Ga-doped magnet (b) and the Zr-doped magnet (c) after GBD at the depth of 0 μm to 300 μm.

Figures 6(b), 6(d), and 6(g) shows the high-magnification EPMA mappings of the Tb distribution of three GBD magnets at the depth of 100 μm. The mapping shows that Tb is mainly distributed along the GB phase and exhibits a dispersion distribution. It is difficult to distinguish the core–shell structure in the original GBD magnet. In addition, the Ga-doped GBD magnet exhibits a discontinuous Tb-rich network. In contrast, the Tb-rich shells of the Zr-doped GBD magnet are complete and continuous. Similar results can be observed in the corresponding SEM in Figs. 6(a), 6(c), and 6(f). Specifically, the concentration and distribution uniformity of Tb in the original GBD magnet, Ga-doped GBD magnet and Zr-doped GBD magnet at the depth of 100 μm are significantly improved in turn. This indicates that Zr doping can effectively optimize the distribution of Tb. The nucleation field of the reversed domain on grain surfaces is enhanced when it is covered by shell, and a complete shell can reduce the nucleation sites.[11]

To understand how the doping elements Ga and Zr affect diffusion depth, the distributions of Ga and Zr were also analyzed via EPMA, as shown in Figs. 6(e) and 6(h). It is found that Ga atoms are distributed in the TJP, as shown in Fig. 6(e). The melting point of Ga is low, which can lower the melting point and improve the fluidity of GB phases. GB phases are the channels for GBD, and the decrease in the melting point of the GB can facilitate the migration of Tb atoms. Similar to the distribution of Ga, Zr also exists in the TJP in the Zr-doped GBD magnet, as shown in Fig. 6(h). Figure 6(i) shows that the B elements are also enriched in the Zr-rich region, indicating the formation of the Zr–B compound, which corresponds to the phase with different contrast in Fig. 4(i) mentioned above.

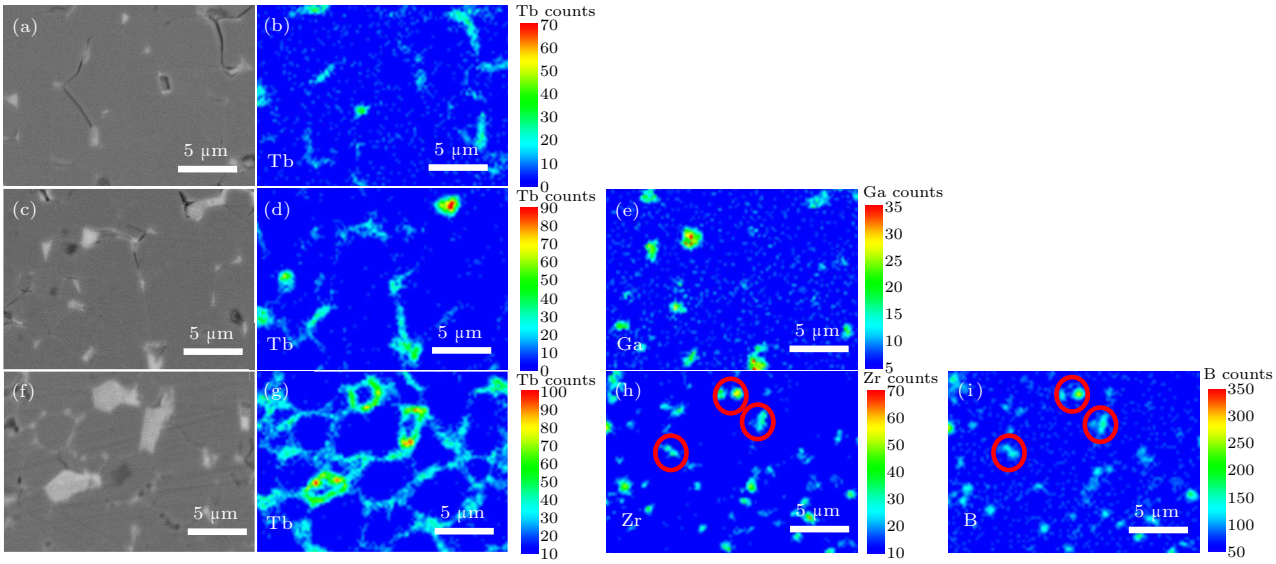


Fig. 6. SEM images [(a), (b), (c)] and EPMA mappings of Tb [(b), (d), (g)], Ga (e), Zr (h), and B (i) of the original GBD magnet, the Ga-doped GBD magnet and the Zr-doped GBD magnet at the depth of 100 μm.

The Zr–B compound in the TJP may be the main reason for the different distribution of Tb. To further analyze the role of Zr–B compounds in the TJP, TEM analysis was performed. Figure 7(a) shows the TJP that contains the Zr–B phase. The Zr–B phase has a strip morphology and is completely encapsulated inside the TJP. According to Fig. 7(b), the selected area electron diffraction (SAED) of the Zr-rich area shows that this area in the TJP is consistent with the structural characteristics of hexagonal ZrB_2, whose melting point is about 3000 °C. Because the formation of ZrB_2 consumes boron, the consumption

of boron leads to the reduction of $Nd_2Fe_{14}B$,[29] thus more GB phases are formed. The distribution of GB phases observed in Figs. 4 and 6 also verifies this result. Therefore, the formation of ZrB_2 can provide a continuous GB structure for GBD. Moreover, we find that ZrB_2 is completely encased in the TJP. There are also many lattice dislocations between the TJP and ZrB_2 phase, as shown in Fig. 7(c), resulting in a high concentration of defects at the interface,[27] which have a high Gibbs free energy. Therefore, Tb atoms need less diffusion activation energy at defect sites, which accelerates atomic diffusion.

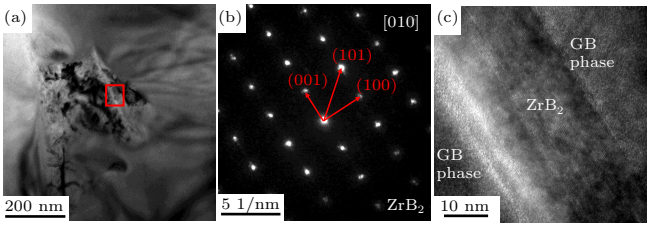


Fig. 7. TEM image of the GB phase of the Zr-doped magnet, and (b) the SAED spot of the corresponding area in the red box of panel (a). (c) High-resolution TEM image of the Zr-doped magnet in the red box area of panel (a).

3.3. Micromagnetic simulation results

Zr doping can significantly increase the diffusion depth, while the shell thickness near the surface also decreases, as shown in Fig. 4. To find out whether the reduction in shell thickness would have a negative effect on coercivity, we carried out a micromagnetic simulation. Figure 8 shows that the coercivity is in accordance with the thickness of the shell. However, the effect of shell thickness on coercivity becomes small when the thickness exceeds 5 nm. In the range of 0 nm to 5 nm, the coercivity increases by 1975 Oe/nm, but by only 425 Oe/nm in the range of 5 nm to 10 nm. According to the simulation results, thin shells are enough to provide a large coercivity increase. The decrease in shell thickness within a certain range does not have a significant negative effect on coercivity. Therefore, the distribution of Tb in the Zr-doped GBD magnet is more advantageous to obtain higher coercivity, i.e., more Tb elements diffusing into the interior of the magnet to form thin shells. With the same amount of the Tb diffusion source (0.42% in this work), the thin shell also means that there can be more Tb surplus to provide the concentration gradient of Tb diffusion to the deeper part of the magnet.

Moreover, the magnetization reversal patterns are shown in Fig. 9. A clear difference can be observed between the magnets before and after GBD. In the model without Tb-rich shells, the magnetic moment begins to reverse at the GB and the edges of the grain surface (blue contrast). In the models with shells, the reversed domains move from the edges of the grain surface to the edge of the core not covered by the Tb-rich shells. The magnetization reversal patterns are also similar for the models with 5 nm shells and 10 nm shells, except that the

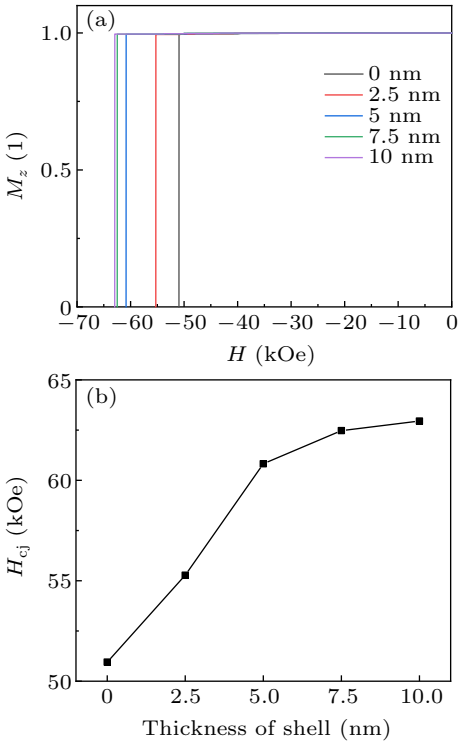


Fig. 8. (a) Demagnetization curves and (b) the coercivity increment for models with shell thicknesses of 0 nm, 2.5 nm, 5 nm, 7.5 nm, and 10 nm, calculated by Magpar.

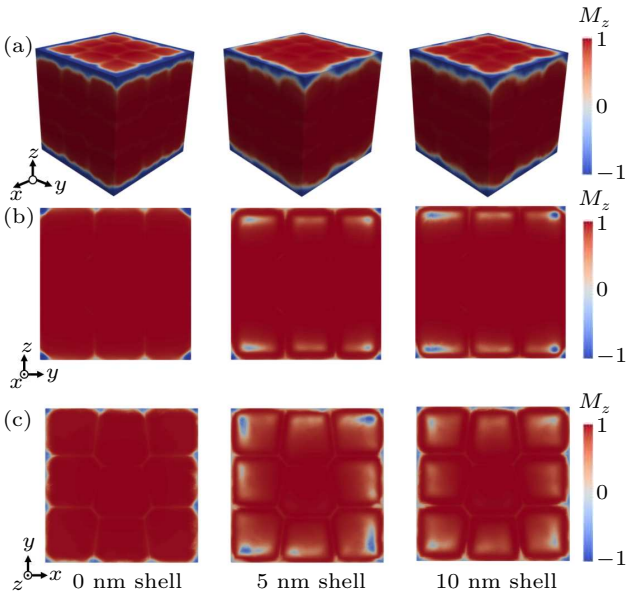


Fig. 9. Magnetization reversal patterns on the outer surfaces (a) and cross-sections of $x = 0.9$ (b) and $z = 0.93$ (c) of models with shell thicknesses of 0 nm, 5 nm, and 10 nm.

nucleation site moves further into the grain in the model with 10 nm shells. Due to the influence of the demagnetizing field, the nucleation field at the grain surface is low. After GBD, the grain surface is covered by Tb-rich shell, which significantly improves the nucleation field at the grain surface. With a further increase in the shell thickness, the nucleation site moves further into the grain. However, from the surface of the magnet to the interior, the demagnetizing field gradually decreases and the distribution of this field inside the magnet is more

uniform.[45] Thus, the nucleation field does not increase much when the nucleation site moves into the grain, which can explain why the coercivity increases little as the shell thickness increases further. Therefore, a 5 nm thin shell is enough to achieve high coercivity. Also, the thicker Tb-shells on the surfaces of the original GBD and Ga-doped GBD magnets result in a waste of Tb.

4. Conclusion

In summary, we found that Ga doping can decrease the melting point and facilitate the fluidity of GB phases, making it easier to form continuous GB phases. Therefore, Ga doping in magnets can slightly improve the coercivity increment by GBD, from 3.24 kOe to 4.32 kOe. The consumption of B in the Zr-doped magnet leads to an increase in the GB phases, which can promote the formation of continuous GB phases. More important is the increase in the defect concentration between ZrB_2 phases and GB phases in the TJP, causing high Gibbs free energy in the TJP, which makes the Tb atoms require less diffusion activation energy during migration. Therefore, Zr doping improves the diffusion depth and uniformity of Tb, which is the direct reason that allows Zr-doped magnets to achieve a 7.97 kOe increment by GBD technology. In the Zr-doped magnet, the increase in diffusion depth will lead to a decrease in shell thickness near the surface. In addition, the reduction in shell thickness within a certain range was found not to have a significant negative effect on coercivity by micromagnetic simulation. This study helps to understand the role of Ga and Zr in the GBD process, and may provide a new perspective for researchers to improve the effects of GBD.

Acknowledgments

Project supported by the National Natural Science Foundation of China (Grant No. 52261037), self-deployed Projects of Ganjiang Innovation Academy, Chinese Academy of Sciences (Grant No. E055B002), the Project of Baotou City Science and Technology (Grant No. XM2022BT04), the Key Research Program of the Chinese Academy of Sciences (Grant No. ZDRW-CN-2021-3) and the Key Research Project of Jiangxi Province (Grant No. 20203ABC28W006).

The authors would like to thank Professor Zhenchen Zhong, Jiangxi University of Science and Technology, for providing guidance for this work.

References

[1] Sagawa M, Fujimura S, Togawa N, Yamamoto H and Matsuura Y 1984 *J. Appl. Phys.* **55** 2083
[2] Dorcec L, Pevec D, Vdovic H, Babic J and Podobnik V 2019 *Journal of Cleaner Production* **210** 887
[3] Hirosawa S, Matsuura Y, Yamamoto H, Fujimura S, Sagawa M and Yamauchi H 1986 *J. Appl. Phys.* **59** 873
[4] Herbst J F 1991 *Rev. Mod. Phys.* **63** 819
[5] Herbst J F and Yelon W B 1985 *J. Appl. Phys.* **57** 2343
[6] Park K T 2000 *Proceedings of 16th International Workshop on Rare Earth Magnets and Their Applications*, 2000, Sendai, Japan, p. 257
[7] Kim T H, Sasaki T T, Koyama T, Fujikawa Y, Miwa M, Enokido Y, Ohkubo T and Hono K 2020 *Scri. Mater.* **178** 433
[8] Löewe K, Brombacher C, Katter M and Gutfleisch O 2015 *Acta Mater.* **83** 248
[9] Hono K and Sepehri-Amin H 2018 *Scri. Mater.* **151** 6
[10] Sugimoto S 2011 *J. Phys. D: Appl. Phys.* **44** 064001
[11] Li J, Sepehri-Amin H, Sasaki T, Ohkubo T and Hono K 2021 *Sci. Technol. Adv. Mat.* **22** 386
[12] Sepehri-Amin H, Ohkubo T and Hono K 2013 *Acta Mater.* **61** 1982
[13] Oono N, Sagawa M, Kasada R, Matsui H and Kimura A 2011 *J. Magn. Magn. Mater.* **323** 297
[14] Liu Z W, He J Y and Ramanujan R V 2021 *Mater. Design* **209** 110004
[15] Zhao L Z, He J Y, Li W, Liu X L, Zhang J, Wen L, Zhang Z H, Hu J W, Zhang J S, Liao X F, Xu K, Fan W B, Song W Y, Yu H Y, Zhong X C, Liu Z W and Zhang X F 2021 *Adv. Funct. Mater.* **32** 2109529
[16] Jin L, Ding G F, Zhu J H, Jin Z H, Zheng B, Guo S, Chen R J, Yan A R and Liu X C 2021 *J. Alloys Compd.* **870** 159375
[17] Zhou T J, Guo Y, Xie G Q, Rehman S U, Liu R H, Liu J R, Qu P P and Li M F 2021 *Intermetallics* **138** 107335
[18] Jin L, Jin Z H, Zhu J H, Ding G F, Zheng B, Guo S, Chen R J, Yan A R and Liu X C 2021 *Chin. Phys. B* **30** 027503
[19] Jin Z H, Ding G F, Fan X D, Cao S, Fan S N, Wang Z X, Zheng B, Guo S, Chen R J, Yan A R and Liu X C 2022 *J. Alloys Compd.* **926** 166725
[20] Zeng H X, Liu Z W, Li W, Zhang J S, Zhao L Z, Zhong X C, Yu H Y and Guo B C 2019 *J. Magn. Magn. Mater.* **471** 97
[21] Li J J, Huang X Y, Zeng L L, Ouyang B, Yu X Q, Yang M N, Yang B, Rawat R S and Zhong Z C 2020 *J. Mater. Sci. Technol.* **41** 81
[22] Wang E H, Xiao C H, He J Y, Lu C F, Hussain M, Tang R H, Zhou Q and Liu Z W 2021 *Appl. Surf. Sci.* **565** 150545
[23] Zhou Q, Liu Z W, Zhong X C and Zhang G Q 2015 *Mater. Design* **86** 114
[24] Chen W, Huang Y L, Luo J M, Hou Y H, Ge X J, Guan Y W, Liu Z W, Zhong Z C and Wang G P 2019 *J. Magn. Magn. Mater.* **476** 134
[25] Bae K H, Lee S R, Kim H J, Lee M W and Jang T S 2015 *J. Appl. Phys.* **118** 203902
[26] Diao S L, Luo Y, Yan W L, Peng H J, Dong Y, Yi H B, Wu S J, Zhang S and Yu D B 2022 *J. Magn. Magn. Mater.* **556** 169429
[27] Zhong S W, Yang M N, Rehman S U, Luo S G, Li L G, Li C, Li J J, Xiong S H, Bulyk I and Yang B 2023 *J. Rare Earth* **41** 1068
[28] Gabay A M, Zhang Y and Hadjipanayis G C 2002 *J. Magn. Magn. Mater.* **238** 226
[29] Shaaban A 2007 *AIP Conf. Proc.* **909** 63
[30] Sasaki T T, Ohkubo T, Takada Y, Sato T, Kato A, Kaneko Y and Hono K 2016 *Scri. Mater.* **113** 218
[31] Huang Q F, Jiang Q Z, Hu J F, Rehman S U, Fu G, Quan Q C, Huang J X, Xu D Q, Chen D K and Zhong Z C 2022 *J. Mater. Sci. Technol.* **106** 236
[32] Zhang Z H, Jin J Y, Liang L P, Peng B X, Liu Y S, Fu S and Yan M 2019 *J. Magn. Magn. Mater.* **487** 165356
[33] Xu F, Wang J, Dong X P, Zhang L T and Wu J S 2011 *J. Alloys Compd.* **509** 7909
[34] Liu D, Ma T Y, Wang L C, Liu Y L, Zhao T Y, Hu F X, Sun J R and Shen B G 2019 *J. Phys. D: Appl. Phys.* **52** 135002
[35] Kim S K, Hwang S and Lee J H 2019 *J. Magn. Magn. Mater.* **486** 165257
[36] Li L, Dong S Z, Chen H S, Jiang R J, Li D, Han R, Zhou D, Zhu M G, Li W and Sun W 2019 *Chin. Phys. B* **28** 037502
[37] Scholz W, Fidler J, Schrefl T, Suess D, Dittrich R, Forster H and Tsiantos V 2003 *Comp. Mater. Sci.* **28** 366
[38] Du Q, Faber V and Gunzburger M 1999 *SIAM Rev.* **41** 637
[39] Quey R, Dawson P R and Barbe F 2011 *Comput. Meth. Appl. M.* **200** 1729
[40] Geuzaine C and Remacle J F 2009 *Int. J. Numer. Meth. Eng.* **79** 1309
[41] Schrefl T, Fischer R, Fidler J and Kronmüller H 1994 *J. Appl. Phys.* **76** 7053
[42] Zhang P Y, Ge H L, Pan M X, Wu Q, Yang H F, Jiao Z W, Gong J and Peng X L 2011 *Adv. Mater. Res.* **179–180** 751
[43] Tsutai A, Sakai I, Mizoguchi T and Inomata K 1987 *Appl. Phys. Lett.* **51** 1043
[44] Zhou S Z and Dong Q F 2004 *Super Permanent Magnets RE-Iron Based Permanent Materials* (Beijing: Metallurgical Industry Press) p. 72 (in Chinese)
[45] Li W, Zhou Q, Zhao L Z, Wang Q X, Zhong X C and Liu Z W 2018 *J. Magn. Magn. Mater.* **451** 704